Structural Design Optimization for CFRP in a Personal Aerial Vehicle

Andrew Hardman[1], Luke Crispo[2], and Tim Sirola[3]
Queen's University, Kingston, Ontario, K7L 3N6, Canada

Jaehyun Ann[4], and Jaewoo Lee[5]
Konkuk University, Seoul, Gyeonggi Province, 05029, Korea

Joon Hyuk Song[6]
KCTECH, Jeonju, Gyeonggi Province, 54853, Korea

Il Yong Kim[7]
Queen's University, Kingston, Ontario, K7L 3N6, Canada

Corresponding Author: kimiy@queensu.ca

Abstract

Increased urban expansion in recent years has uncovered an inefficiency in mid-range travel distances between 80km and 800km. Urban Air Mobility (UAM) aims to address this gap using hybrid and full-electric Personal Air Vehicles (PAVs) as a source of accessible, on-demand transportation. To achieve success with PAVs, reduction of mass is imperative due to the current battery capacity constraints. This can be achieved using advanced materials such as Carbon Fibre Reinforced Polymers (CFRPs) paired with advanced design tools such as topology and composite optimization. Presently, existing literature in UAM design is focused on conceptual design optimization with high-level structural considerations for only conventional materials, which leaves significant weight savings unrealized. This work addresses this knowledge gap by presenting a structural optimization methodology for CFRP based UAM design applied to a PAV concept created in collaboration with Queen's University, Konkuk University, and KCTECH. A comparison between a CFRP and a conventional aluminum design shows a mass reduction of 54.1% using CFRP construction while meeting the same design requirements.

I. Introduction

Rapid urbanization in recent years has contributed to an increasing need for on-demand transportation over mid-range distances (80-800km), which is inherently inefficient when using traditional road, rail, or air vehicles [1]. Urban Air Mobility (UAM) is a disruptive concept that aims to address this gap using Personal Air Vehicles (PAVs) as a source of accessible, on-demand transportation. Previously, several limitations prohibited significant development of UAM, however recent technological advances and depleting resource availability make now the right time to explore

[1] MASc Student, Department of Mechanical and Materials Engineering, Queen's University
[2] PhD Student, Department of Mechanical and Materials Engineering, Queen's University, 1025655
[3] MASc Student, Department of Mechanical and Materials Engineering, Queen's University
[4] MASc Student, Aerospace Design-Airworthiness Institute, Konkuk University
[5] Professor, Aerospace Design-Airworthiness Institute, Konkuk University
[6] Director, Composite Engineering Center, Korea Institute of Carbon Convergence Technology
[7] Professor, Department of Mechanical and Materials Engineering, Queen's University

This is the pre-print version of the following article: https://arc.aiaa.org/doi/10.2514/6.2021-3067, which has been published in final form at https://doi.org/10.2514/6.2021-3067.

these transformative aircraft technologies [2]. Hundreds of startups and established aerospace companies are currently developing PAV concepts, with almost all using battery or hybrid-electric power sources. Given energy density constraints associated with current battery technology [3], the reduction of structural mass in PAVs, while meeting all necessary performance and safety requirements, is imperative to achieving success in future UAM design. Computational design optimization techniques and advanced composite materials are both promising avenues for realizing this goal.

Topology Optimization (TO) is a numerical design tool used to determine an optimum distribution of material within a given design domain to maximize a performance measure subject to design constraints. TO has been effectively applied to develop lightweight structures in the aerospace industry [4], with Krog et al. achieving an empty mass reduction of 0.36% in the Airbus A380 by optimizing leading edge ribs [5], Wong et al. reducing mass of a landing gear assembly under dynamic loading by 36% [6], and Trivers et al. optimizing a business aircraft seat for a mass reduction of 32% [7]. Other design optimization techniques, such as size or shape optimization can be used as additional steps to further fine tune geometry [8].

The use of advanced composites, such as Carbon Fibre Reinforced Polymers (CFRP), in mechanical design can enable significant weight savings due to their high stiffness-to-weight ratio when compared to conventional aerospace materials, such as aluminum. Recent research has incorporated advanced composites into computational design optimization and has shown to be effective in further reducing mass. Shrivastava et al. [9] proposed a multi-objective, multi-laminate design optimization methodology for composite structures using genetic algorithms. This approach was applied to the design of a wing torsion box showing a 54% reduction in mass compared to an aluminum design. Kupchanko et al. [10] applied a topology and CFRP laminate optimization approach in Altair OptiStruct to reduce the compliance of an aircraft seat by 8% relative to an aluminum 2024 design of the same mass.

Recent publications in PAV conceptual design have shown performance improvements through the implementation of conceptual design optimization methodologies. Clarke et al. [3] proposed several potential multidisciplinary conceptual design optimization approaches for minimising the maximum takeoff weight (MTOW), mission time, and energy consumption. Optimization for mass yielded a reduction in MTOW (9.2%), battery energy consumption reductions (10.8%), and total mission time (3.3%). Hendricks et al. [11] presented a multidisciplinary optimization methodology for PAV design using NASA's OpenMDAO framework with the objective of reducing initial fuel mass. This was applied by changing multi-disciplinary conceptual design variables such as propeller speed, wingspan, wing twist, and cruise altitude subject to structural, propulsion and trajectory constraints. Optimization yielded a fuel consumption reduction of 15.5%. Presently, existing literature on PAV design is focused on conceptual design optimization with high-level structural considerations. By focusing purely on high-level conceptual design parameters and considering only conventional structural materials, these approaches leave significant weight savings unrealized.

The objective of this work is to present a structural optimization approach for detailed PAV design and to apply the method on a PAV concept created in collaboration with Queen's University, Konkuk University, and the Korea Institute of Carbon Convergence Technology (KCTECH). A representative Finite Element Analysis (FEA) model is presented and subjected to realistic loading conditions selected from the flight envelope determined for this PAV concept. Based on this FEA model, two PAV designs are optimized using primarily CFRP or primarily aluminum, respectively, such that they can be compared in terms of mass, stiffness, and strength. This research will demonstrate the applicability of topology optimization to UAM and investigate the benefits of CFRP and aluminum construction as it pertains to PAV design.

II. Modelling

A. Structural Design

This work's structural analysis and optimization is based on a hybrid electric vertical takeoff and lift (VTOL) PAV design concept created in collaboration with Queen's University, Konkuk University, and KCTECH. The design concept features an internally reinforced skin design with stringers and frames in the fuselage, and ribs and spars in the wing. The baseline wing geometry has twin continuous I-beam spars in a box wing configuration, with I-beam ribs placed at an interval of 300mm apart tangent to the skin. The fuselage consists of 8 stringers and 25 frames, with four frames being directly joined to the wing spars to connect the fuselage to the wing. Four tilting VTOL and cruise propulsors are attached to twin booms mounted between two ribs and the spars. Figure 1a shows the full geometry with the external skin and Figure 1b shows the full geometry without the skin to reveal the internal structure. A breakdown of the individual components for the fuselage and wings are shown in Figure 2 and Figure 3, respectively.

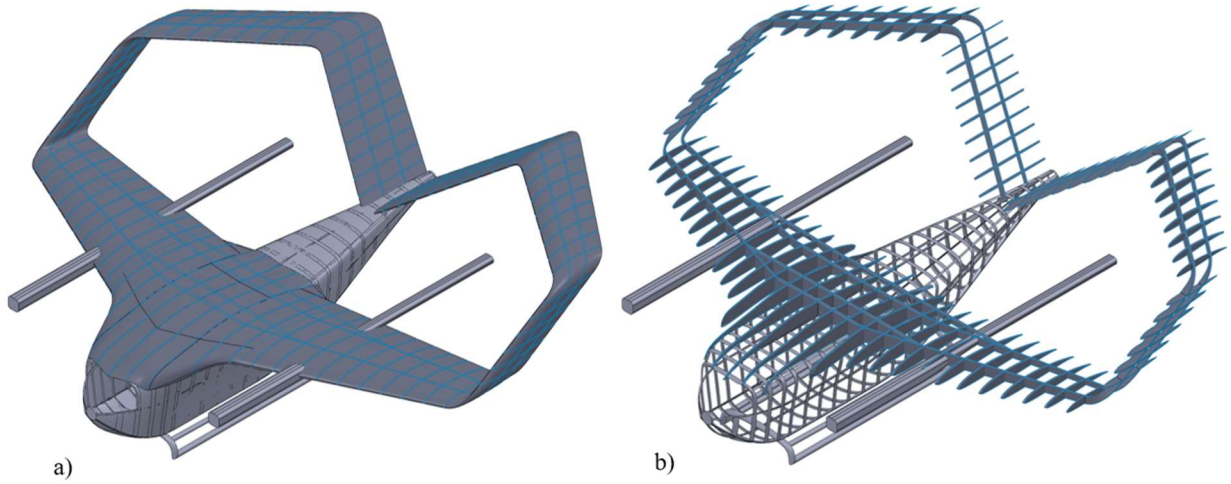

Figure 1: Isometric view of the initial airframe geometry a) with skin and b) without skin to show the ribs, spars, frames, and stringers.

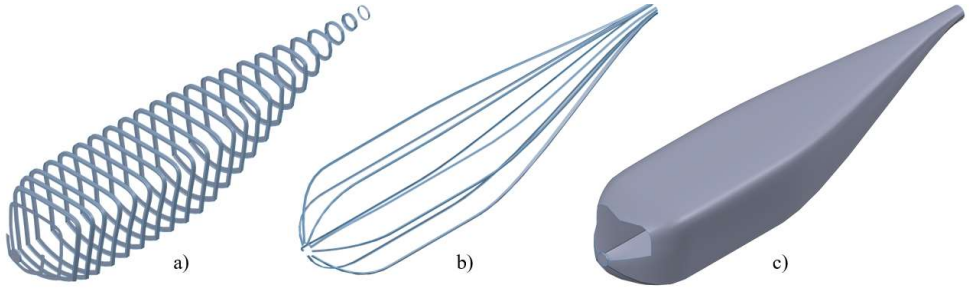

Figure 2: Three groups of components making up the fuselage structure: a) Frames, b) Stringers, c) Skin.

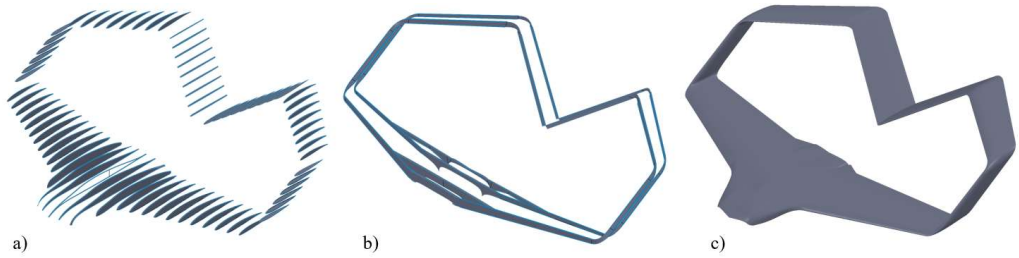

Figure 3: Three groups of components making up the wing structure: a) Ribs, b) Spars, c) Skin.

B. Materials

The alloy chosen for the aluminum design is Aluminum 2024 – T4 due to its wide use in the aerospace industry in sheet form. For the composite design, the external skin of the fuselage and wings presents an excellent opportunity to use a laminated CFRP material due to large panel areas. A high-performance woven fabric prepreg CFRP material developed by KCTECH offers superior stiffness-to-weight performance relative to aluminum. The internal structures of the wing and fuselage require complex geometries, therefore a laminated CFRP construction is not feasible. Long Fibre Prepreg Sheet (LFPS) is used for the internal structure of the composite design. LFPS is a composite material developed by KCTECH consisting of 50mm long carbon fibres and epoxy resin formed using a hot compression moulding process allowing for more complex geometries. Table 1 presents a summary of material properties for Aluminum – 2024, LFPS, and the KCTECH woven fabric prepreg.

Table 1: Properties of chosen PAV construction materials, where E_{11}, E_{22} are the Young's Moduli in the 1st and 2nd principal directions, respectively.

Material Property	Aluminum 2024 – T4 [12]	LFPS [13]	Woven Fabric Prepreg [13]
E_{11}, E_{22} [GPa]	73	37.9	69.38
Tensile Strength [MPa]	325	345.6	1115
Compressive Strength [MPa]	325	318	800
Shear Strength [MPa]	325	89.1	59.32
Density [g/cm^3]	2.78	1.56	1.5
Application	All components	Interior Components (Ribs, Spars, Stringers, Frames)	Exterior Components (Skin)

The Tsai-Wu composite failure criterion is chosen to predict failure of the LFPS and Woven Fabric Prepreg materials, while the Von-Mises failure criterion is chosen to predict material failure for the aluminum design. The Tsai-Wu failure theory uses multiple strength parameters to predict failure based on directional stresses. Failure is predicted when the composite failure index reaches 1, which is described mathematically in Eq. (1):

$$F_i\sigma_i + F_{ij}\sigma_i\sigma_j \le 1 \quad \text{for } i, j = 1,...,6 \tag{1}$$

where F is the tensor of determined material strength parameters and σ is the vector of measured stresses. For the woven fabric prepreg material used in this study, Eq. (1) can be written in terms of the strength input variables (listed in Table 1) as follows in Eq. (2):

$$\left(\frac{1}{X_T} - \frac{1}{X_C}\right)\sigma_1 + \left(\frac{1}{Y_T} - \frac{1}{Y_C}\right)\sigma_2 + \frac{\sigma_1^2}{X_T X_C} + \frac{\sigma_2^2}{Y_T Y_C} + \frac{\sigma_6^2}{S^2} + 2S\sigma_1\sigma_2 \le 1 \tag{2}$$

where X_T, Y_T are the tensile strengths in the 1st and 2nd principal directions respectively, X_C, Y_C are the compressive strengths in the 1st and 2nd principal directions respectively, S is the shear strength in plane, σ_1, σ_2 are the stresses in the 1st and 2nd principal directions respectively, and σ_6 is the shear stress in plane.

C. Load Cases

Figure 4 shows the flight envelope generated during the conceptual design phase of the PAV design used for this paper. Three ultimate load cases are defined, where LC1 is the highest possible load factor (4.552), LC2 is the highest possible speed at the maximum load factor (3.800), and LC3 is the highest possible speed at the minimum load factor (-1.552). Table 2 shows the resultant load cases determined from the flight envelope diagram.

Table 2: Ultimate Load Cases for Fixed Wing Flight.

Load Case	Lift Force (kN)	Load Factor (g)	Speed (m/s)	Dynamic Pressure due to speed (Pa)	Angle of Attack (deg)
1	69.94	4.552	61.73	2286	12.44
2	53.39	3.800	84.52	4286	3.313
3	-23.36	-1.552	84.52	4286	-6.659

When applied to the FEA models, each ultimate load case is accompanied by two additional variants – one with 15 degrees roll and sideslip angle, and another with -15 degrees roll and sideslip angle. An additional set of loading cases are taken from regulatory emergency load cases for commuter category airplanes and are shown in Table 3 [14].

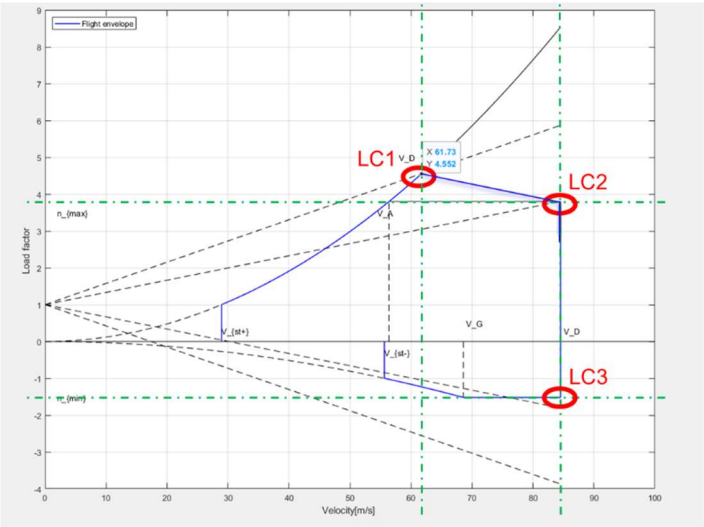

Figure 4: Flight envelope (V-n) diagram showing the 3 ultimate load cases for Fixed Wing Flight.

Table 3: Emergency Load Cases defined by [14].

Load Case	Inertial Load Direction	Magnitude (g)
1	Upward	3.0
2	Downward	6.0
3	Forward	18.0
4	Left	4.5
5	Right	4.5

D. FEA Models

The full airframe is modelled within the Altair HyperWorks suite as two separate FEA simulations: 1) wings with booms and 2) fuselage, with boundary conditions applied to simulate the full airframe encountering the same load cases. The connection between the wing and fuselage structure is applied as fixed displacement boundary conditions to both models. To simulate the adhesion between internal components (frames, stringers, ribs, spars) and the skin, a FREEZE contact definition is used. This creates an ideal bond between two surfaces, allowing for no separation or compliance. This necessary simplification requires a conservative safety factor to be applied to the optimization results, as this contact scenario will predict superior performance relative to a real adhesive or rivet joint.

1. Fuselage Model

In addition to the ultimate and emergency loads, forces are applied at the landing gear attachment points to simulate the load transferred from the landing gear during a hard 5g landing. Details of the fuselage landing gear loads are summarized in Table 4. A total of 15 load cases are applied to the wing model (9 ultimate loads, 5 emergency loads, and 1 landing load).

Table 4: Additional fuselage load case to simulate hard landing loads from the landing gear.

Load Case	Front Landing Gear Attachment Load (N)			Rear Landing Gear Attachment Load (N)		
	X	**Y**	**Z**	**X**	**Y**	**Z**
15	0.0	18393.8	0.0	0.0	18393.8	0.0

Since only half of the geometry is modelled, boundary conditions are applied along the axis of symmetry to prevent z-translation and x-rotation as shown in Figure 5a. In addition to the symmetry boundary conditions, regions along the top of the fuselage that correspond to the attachment points of the wing structure are constrained in all degrees of freedom (DOF). Dynamic pressures due to speed loading (blue) are applied to all skin elements along the front cross section of the fuselage. Components of significant mass (passengers, fuel cells, and batteries) are modelled as concentrated mass (CONM2) elements and joined to the structure with interpolation elements (shown in red in Figure 5b). All inertial loads are applied as accelerations at the fuselage centre of gravity (CG). The hard landing forces

(black) are transmitted to nodes on the appropriate frames in the attachment regions using interpolation (RBE3) elements.

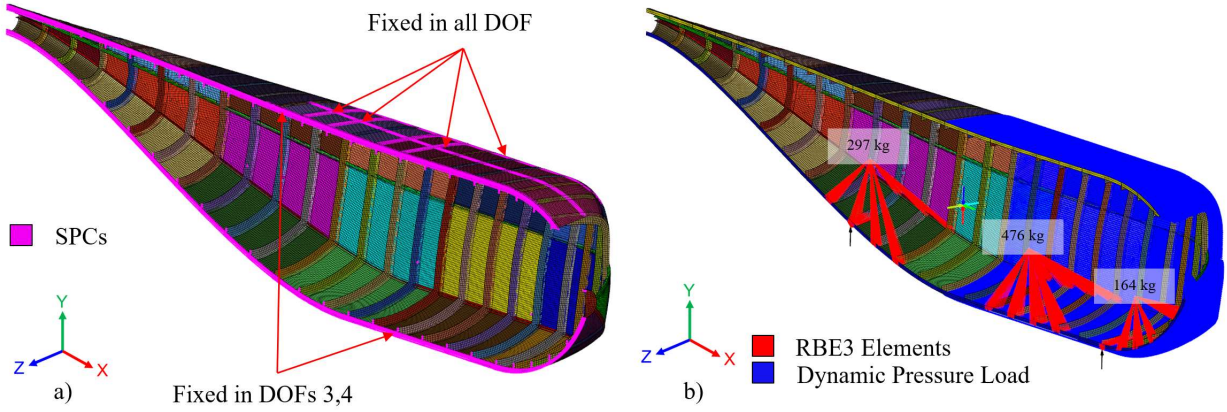

Figure 5: Diagram showing a) the boundary conditions and b) the loads applied to the fuselage model.

2. Wing Model

In addition to the ultimate and emergency loads, three load cases are added in Table 5 to simulate the VTOL function of the PAV. The first load cases has the maximum thrust of all motors applied upwards and the two additional cases have 1 motor shut off due to a failure. A total of 17 load cases are applied to the wing model (9 ultimate loads, 5 emergency loads, and 3 boom loads).

Table 5: Boom lift load cases applied to the wing model in addition to the ultimate and emergency load cases.

Load Case	Force – Front Motor (N)			Force – Rear Motor (N)		
	X	Y	Z	X	Y	Z
15	-	5518	-	-	5518	-
16	-	-	-	-	5518	-
17	-	5518	-	-	-	-

Figure 6a shows the boundary conditions applied to the wing model. The wings are fixed in all degrees of freedom on the attachment points between the fuselage and wings. Due to the symmetry of the wing geometry, the wing is modelled with half symmetry about the X-Y plane, therefore points on that plane are fixed in the Z direction for continuity. Figure 6b shows the loads applied to the wing model. For each of the ultimate load cases, the lift force is resolved as a pressure load (lift pressure), applied across the horizontal wing sections, and dynamic pressure due to speed is applied at all forward-facing wing sections. The inertial loads (load factor, emergency loads) are applied to the CG, and the boom lift loads are applied to the ends of the boom as forces.

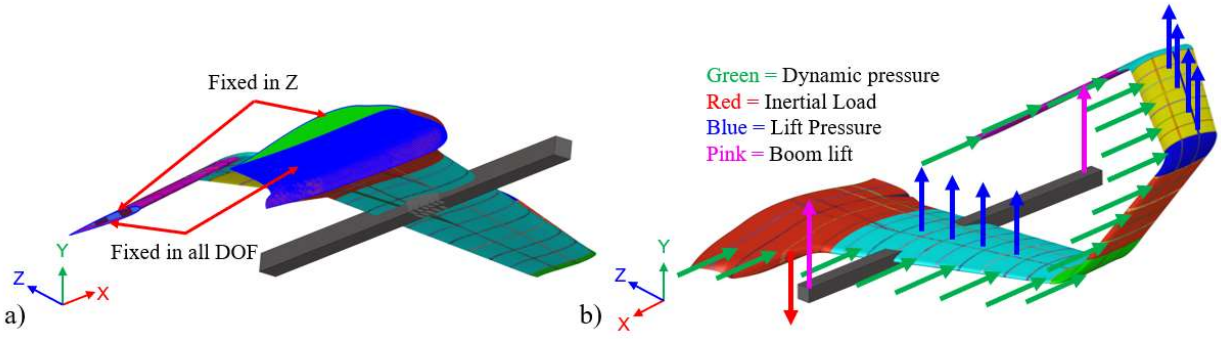

Figure 6: Diagram showing a) the boundary conditions and b) the loads applied to the wing model.

III. Optimization Methodology

Throughout the design process, multiple optimization types of are leveraged depending on the structures and/or materials under consideration. The general flow of the procedure followed during the PAV structural optimization is shown in Figure 7.

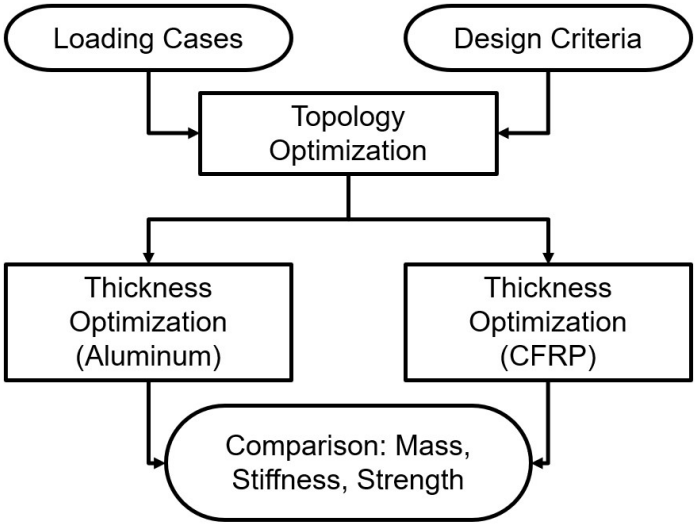

Figure 7 : Design optimization process flow chart.

First, a topology optimization of the internal wing structures is conducted to reduce structural mass by removing unnecessary material from the rib and spar structures. After the topology optimization, a reinterpreted CAD model of the wing structure is generated to perform subsequent sizing optimizations. Following the topology optimization, thickness optimization is performed on all structural components. In this stage, two different types of size optimization are utilized based on the material considered in the model. Gauge optimization is used for both aluminum and LFPS materials to optimize thickness on a component level. For the Woven Fabric Prepreg material, laminate optimization is used to optimize the thickness of individual plies within the laminate. This method is selected due to its ability to consider the orientation of the fibers in each ply throughout the optimization process. As shown in Figure 7, the aluminum and composite models are considered independently throughout the design process. This allows for a direct comparison of each optimized design in terms of mass, stiffness, and strength.

A. Topology Optimization

Topology optimization is a FE-based design tool that uses the existence of elements to determine geometry. An element's existence (or lack thereof) is indicated by its density on a scale from 0 to 1 – where 0 indicates a "void" element that contributes zero mass and stiffness, and 1 indicates a "full" element that contributes the nominal mass and stiffness of the material. Figure 8 provides a simplified example of topology optimization. The element density design variable is continuous, and therefore intermediate densities are possible, which are modelled to contribute intermediate mass and stiffness to the design. Topology optimization is used as the first step in the wing structural optimization to determine the optimal cutouts within the ribs and spars.

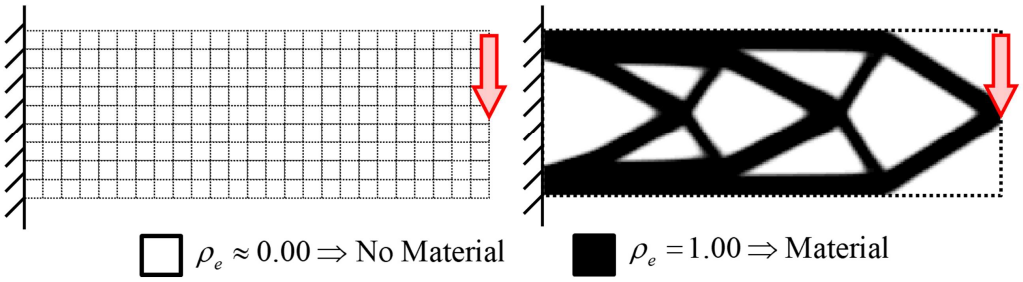

Figure 8: Example of topology optimization applied to a simple geometry.

B. Aluminum Thickness Optimization

Gauge optimization, a form of size optimization, is used for all aluminum components to optimize the thickness, or gauge, of a component. This type of optimization is confined to 2D elements (shells) and considers the FEA model's property thickness as a design variable. This method is preferable to free size optimization as it results in uniform optimized thickness at the component level, as opposed to the individual element level, which drastically reduces the complexity of the design interpretation required for manufacturability. The internal structural components considered in this design (I-beams and thin sheets) are ideal candidates for gauge optimization as they are modelled with 2D shell elements and have discrete manufacturable thicknesses.

C. Composite Thickness Optimization

The composite thickness optimization methodology for this project involves two separate algorithms for the two different materials considered (LFPS and Woven Fabric Prepreg). The Woven Fabric Prepreg material consists of strong, stiff, but brittle woven carbon strands held within a matrix of weak, but more ductile polymer resin. The resin matrix acts to reduce brittleness of the composite material while the carbon strands provide superior strength and stiffness along their axes. If forces are applied along the carbon strands of the CFRP, it is very nearly as stiff/strong as the bare carbon strands, but if forces are applied at an angle to the carbon strands, the stiffness and strength is reduced. A structurally optimal CFRP component will therefore transfer loads along the axes of the carbon strands. When performing composite optimization with directional materials, the optimizer should both vary the thickness and the fiber orientation within each element to achieve the best strength/stiffness for all loads in the structure. In FEA, multi-ply composite laminates are modelled as a single element with multiple layers (plies) of different fiber orientations. The chosen optimization method for Woven Fabric Prepreg material (laminate optimization) varies the thickness of individual plies within a laminate to optimize the chosen design objective. The thickness of each ply is constant across the entire component, like gauge optimization. The thickness of each ply is discretized into multiples of the user-defined ply thickness to ensure manufacturability. The total laminate thickness is also controlled by a user-defined minimum and maximum thickness. Figure 9 shows an example of this process, where the initial design has an equal thickness for both orientations (each 2.40mm or 12 plies of 0.20mm thickness), and the optimized design has different thicknesses for the two orientations (3.20mm or 16 plies for 0 degrees, 0.60mm or 3 plies for 45 degrees).

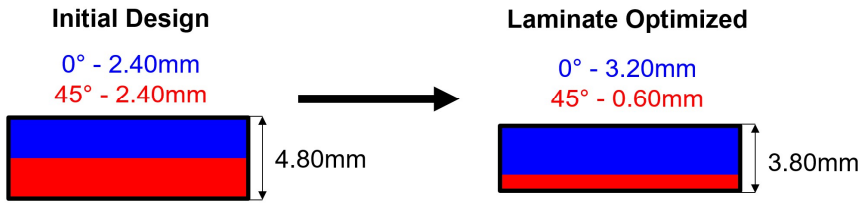

Figure 9: Simplified example of a component being optimized using the laminate optimization methodology.

The LFPS material is assumed to be in-plane isotropic due to the random nature of the carbon strands, and therefore the material properties are not variable via fiber orientations. Thus, gauge thickness optimization can be used for components with this material. The total element thickness is discretized into multiples of user-defined ply thickness to ensure manufacturability.

IV. Optimization Setup

A. Topology Optimization

Topology optimization is implemented as a compliance minimization problem with a constraint on the maximum volume fraction of the final optimized topology (75%) with the following problem statement shown in Eq. (3):

$$\text{minimize:} \quad \text{compliance}(\underset{\sim}{\rho}) \tag{3}$$

$$\text{subject to:} \quad \frac{\sum_i \rho_i v_i}{\sum_i v_i} \leq 0.75$$

$$\underset{\sim}{\underset{\sim}{K}}\,\underset{\sim}{u} = \underset{\sim}{f} \qquad \text{for linear static problems}$$

$$\forall \text{ element } i, \rho_i \in (0,1] \quad \text{where } i = 1,\ldots,68881 \text{ designable elements}$$

where ρ_i is the density of a given element i, v_i is the volume of a given element i, $\underset{\sim}{K}$ is the stiffness matrix for each linear static problem, $\underset{\sim}{u}$ is the displacement vector, and $\underset{\sim}{f}$ is the vector of external forces.

In the wing design optimization, topology optimization is conducted for the webs of the ribs and spars. An image of the components considered in the topology optimization is shown in Figure 10. All rib webs are treated as a single design space, such that a variable amount of material can exist for each (including no material if their structural contribution is minimal), allowing for more design freedom. Each spar is treated as an individual design space to ensure both spars have similar sized cutouts.

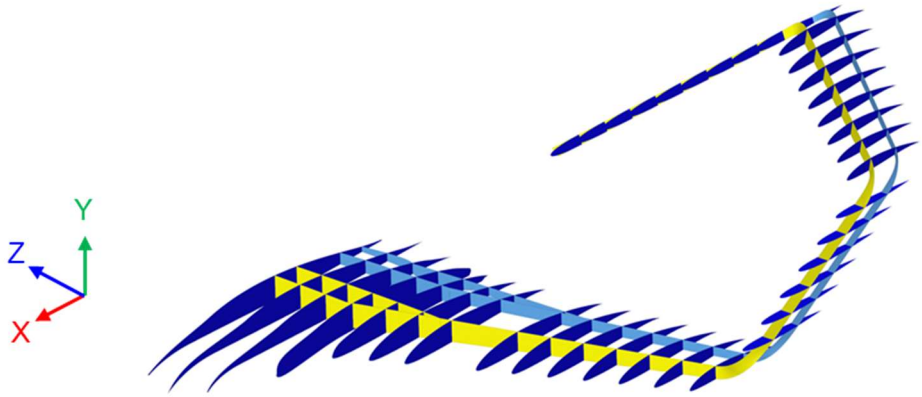

Figure 10: Components considered for topology optimization.

B. Thickness Optimization

Figure 11 and Figure 12 show the individual components (represented by different colours) considered in the thickness optimization for the wing and fuselage models respectively.

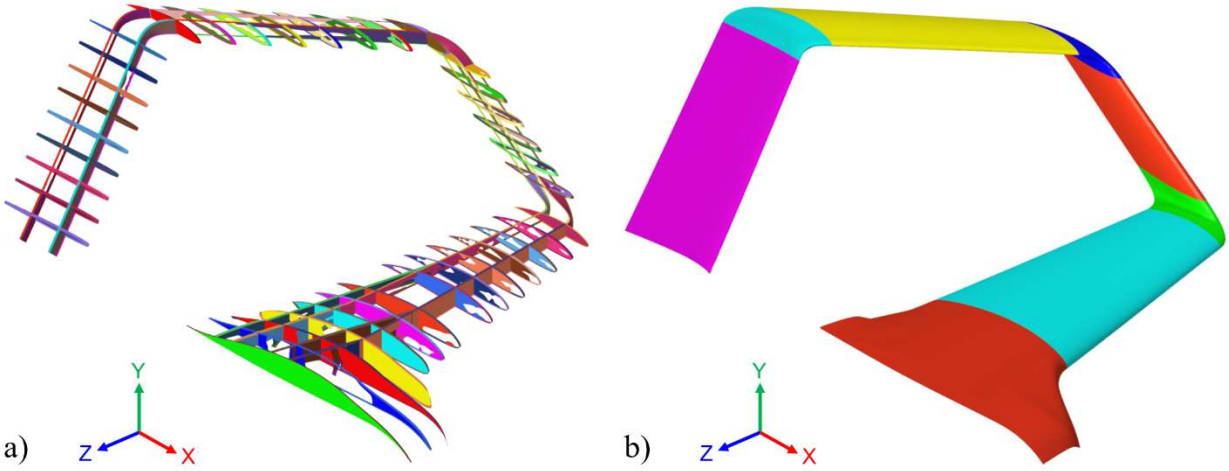

Figure 11: a) Wing model internal components after topology optimization considered for thickness optimization, b) Wing model external skin considered for thickness optimization.

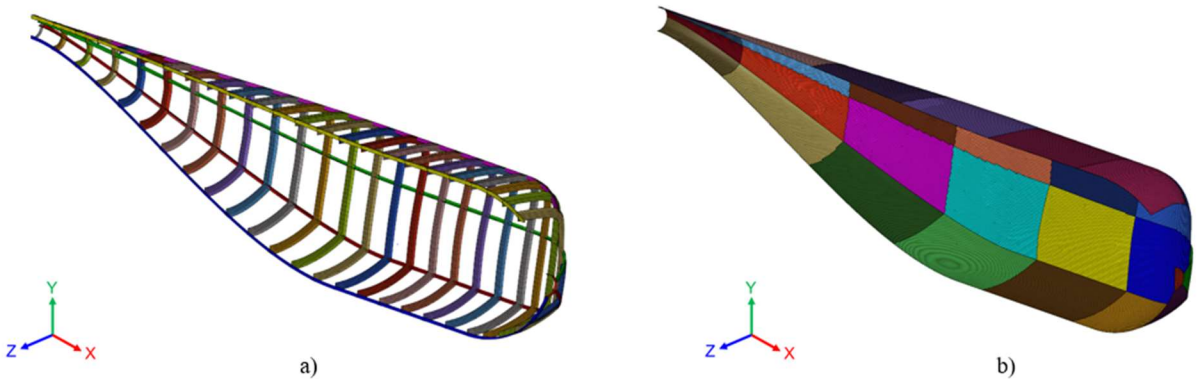

Figure 12: a) Fuselage model internal components considered for thickness optimization, b) Fuselage model external skin considered for thickness optimization.

The fuselage and wing models share the same problem statements but contain different numbers of load cases, laminates, and components, specified by Table 6.

Table 6: Size optimization specifications.

	Wing Optimization	**Fuselage Optimization**
Load Cases (N)	17	15
CFRP Prepreg Laminates (L)	8	28
LFPS Components (M)	117	58
Aluminum Components (M)	125	86

1. Aluminum Gauge Thickness Optimization

Aluminum gauge optimization is performed on all components shown in Figure 11 and listed in Table 6 using a discrete set of common gauge sizes for sheet aluminum with the following mathematical problem statement, eq. (4):

$$\begin{aligned} &\text{Minimize:} && \text{mass}\left(\underset{\sim}{t}\right) && && (4)\\ &\text{Subject to:} && \sigma_i \le 230.75 \text{ MPa} && \text{i} = 1,\ldots\text{N load cases}\\ & && \underset{\sim}{K}\underset{\sim}{u} = \underset{\sim}{f} && \text{for linear static problems}\\ & && t_j \in \{1.016, 1.270, 1.600, 1.803, 2.032, && \\ & && \quad 2.286, 3.175, 4.064, 4.826, 6.350\} \text{ mm} && \text{j} = 1,\ldots,\text{M components} \end{aligned}$$

where σ_i is the maximum Von-Mises stress for the ith load case and t_j is the gauge thickness of the jth component.

2. Composite Sizing Optimization

The Woven Fabric Prepreg external skin components for the wing and fuselage models, shown in Figure 11b and Figure 12b respectively and listed in Table 6, are optimized using the laminate optimization methodology. The Woven Fabric Prepreg laminates are initialized with 2 ply bundles of 2.4mm thickness – one with a 0-degree fiber orientation, and the other with a 45-degree fiber orientation. Each ply bundle is modelled as multiple plies each with a thickness of 0.2 mm – the thickness of each ply bundle is therefore confined to be multiples of 0.2mm. A minimum of 3 plies and maximum of 25 plies per laminate results in a minimum and maximum Woven Fabric Prepreg laminate thickness of 0.6mm and 5.0mm, respectively. The LFPS internal structural components for the wing and fuselage models, shown in Figure 11a and Figure 12a respectively and listed in Table 6, are optimized using the gauge optimization methodology. Each ply of LFPS material has a thickness of 0.7 mm, therefore the overall thickness of each component is confined to be multiples of 0.7mm. A minimum of 3 plies and maximum of 25 plies results in a minimum and maximum LFPS laminate thickness of 2.1mm and 17.5mm, respectively. Sizing optimization (gauge and laminate) is performed simultaneously on all composite components (LFPS and CFRP Prepreg) using the following mathematical problem statement, Eq. (5):

Minimize:	$\text{mass}\left(\underset{\sim}{t}_{LFPS}, \underset{\sim}{t}_{ply}\right)$		(5)
Subject to:	$CFI_i \le 0.5$	i = 1,…N load cases	
	$\underset{\sim}{K}\underset{\sim}{u} = \underset{\sim}{f}$	for linear static problems	
	$2.1\text{mm} \le t_{LFPS,j} \le 17.5\text{mm},\ \Delta t = 0.7\text{mm}$	j = 1,…,M components	
	$0.0\text{mm} \le t_{bundle,k} \le 5.0\text{mm},\ \Delta t_{bundle} = 0.2\text{mm}$	k = 1,2 plies per laminate	
	$t_{lam,l} = \sum_{j=1}^{2} t_{bundle,k}$		
	$0.6\text{mm} \le t_{lam,l} \le 5.0\text{mm},\ \Delta t_{lam} = 0.2\text{mm}$	l = 1,…,L laminates	

where CFI_i is the maximum Tsai-Wu composite failure index for the i[th] load case, $t_{LFPS,j}$ is the thickness of the j[th] LFPS component [mm], $t_{ply,k}$ is the thickness of the k[th] ply of a given laminate [mm], and $t_{lam,l}$ is the thickness of the l[th] prepreg CFRP laminate [mm].

V. Results

A. Topology Optimization

An optimized topological density contour plot of the wing structure is shown in Figure 13.

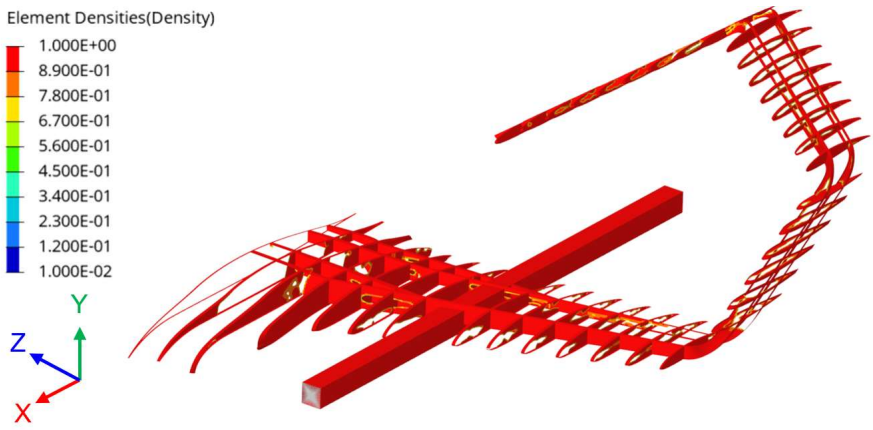

Figure 13: Topological density contour plot and associated scale of the wing structure without skin, showing element densities above 0.8.

The ribs and spars in the lower main wing section have much of the original elements remaining due to the large lift loads applied to the wing surface. Conversely, the ribs and spars in the side vertical wing section are mostly void elements due to the smaller loads and because the skin carries more of the load in-plane as opposed to in-bending for the horizontal sections. After topology optimization, an interpretation of the results is required to perform further analysis and optimization. Elements with densities above 0.8 are overlayed on the original CAD of the wing, such that cuts can be made to the geometry and be re-meshed for subsequent optimization.

B. Aluminum Gauge Optimization

The aluminum optimized thickness results for the fuselage stringers/frames and the skin are shown in Figure 14a and Figure 14b respectively.

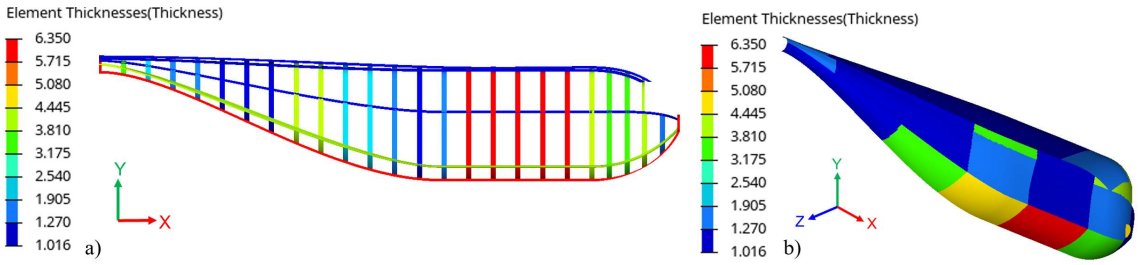

Figure 14: Contour plot and associated scale [mm] of the fuselage aluminum thickness optimization result for the a) stringers and frames and b) skin.

Figure 14 shows that the maximum thickness of aluminum fuselage components occurs in the frames that are connected to the wings (via boundary conditions) and to which the majority of the internal component mass elements are attached. Most components and panels in the rear section of the fuselage go to the minimum thickness due to a lack of load transfer.

The aluminum optimized thickness results for the wing ribs/spars and the skin are shown in Figure 15a and Figure 15b respectively.

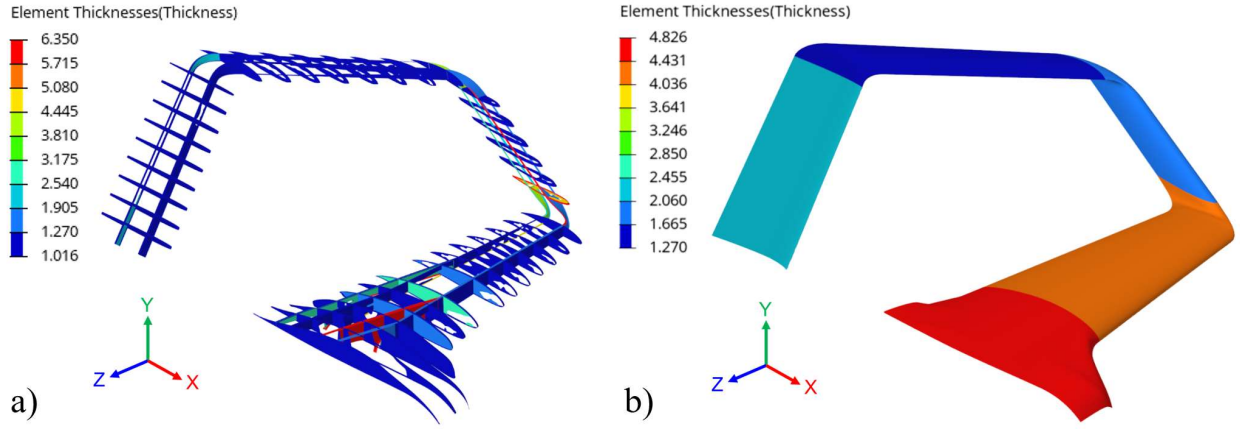

Figure 15: Contour plot and associated scale [mm] of the wing aluminum thickness optimization result for the a) ribs and spars and b) skin.

Figure 15 shows that a significant portion of the internal structural components in the aluminum optimized wing design, as well as the top skin section, are the minimum thickness (1.016mm). The fore-spar is the only component that reaches the maximum thickness, which is to be expected given that a significant amount of the lift load is transferred through that component.

C. Composite Optimization

The composite optimized thickness results for the fuselage stringers/frames and the skin are shown in Figure 16a and Figure 16b respectively.

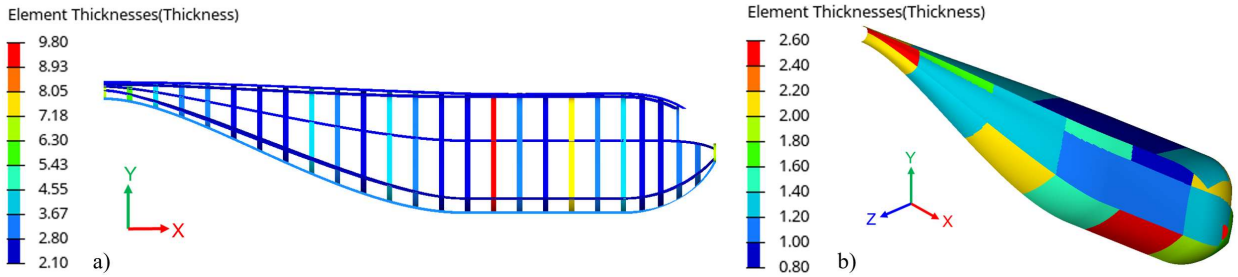

Figure 16: Contour plot and associated scale [mm] of the fuselage composite optimization result for the a) stringers and frames and b) skin.

Figure 16 shows that the maximum thickness of composite fuselage components occurs in the frames connected to the wings (via boundary conditions) and to which the majority of the internal component mass elements are attached.

The individual orientation thicknesses for the composite fuselage optimized design skin are shown in Figure 17.

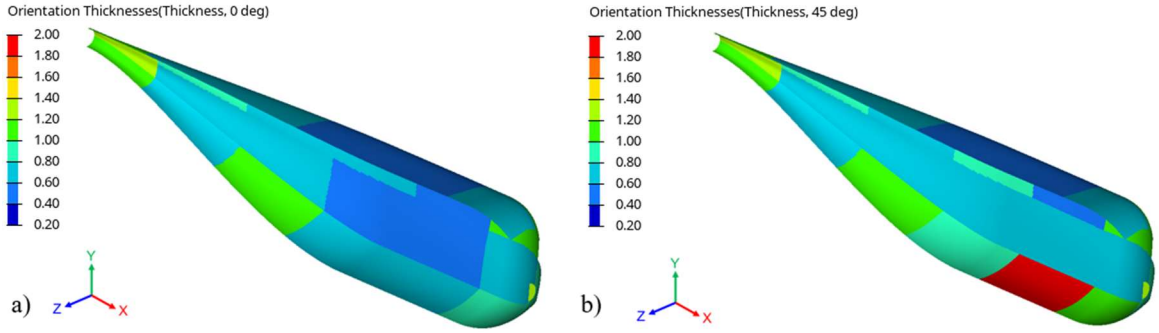

Figure 17: Contour plot and associated scale [mm] of the ply orientation thicknesses resultant from the fuselage laminate optimization. 0 degrees is shown in a) and 45 degrees is shown in b).

The distribution of thickness in the composite fuselage skin is similar for both the 0-degree and 45-degree orientations, apart from the bottom layer where the internal component masses are present. This increased thickness is likely due to the emergency loads, which impart off-angle forces due to inertial loads on the mass elements.

The composite optimized thicknesses for the wing ribs/spars and skin are shown in Figure 18a and Figure 18b, respectively.

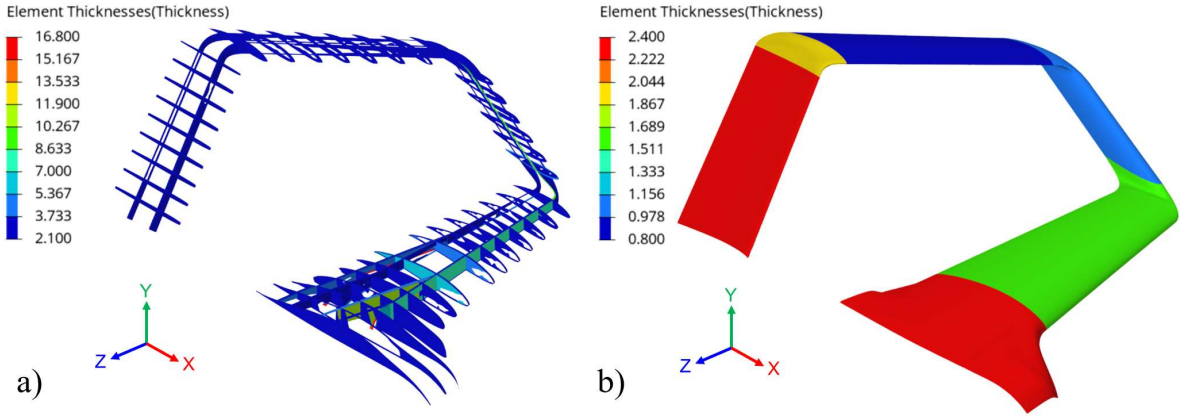

Figure 18: Contour plot and associated scale [mm] of the wing composite optimization result for the a) ribs and spars and b) skin.

As with the aluminum design Figure 18 shows that a significant portion of the internal structural components in the CFRP wing optimized design are the minimum thickness (2.10mm). No skin components reach the maximum allowed thickness for the woven fabric prepreg material (5.00mm), with the maximum being 2.40mm in the skin sections which are joined to the fuselage (via boundary conditions).

The individual orientation thicknesses for the CFRP wing optimized design skin are shown in Figure 19.

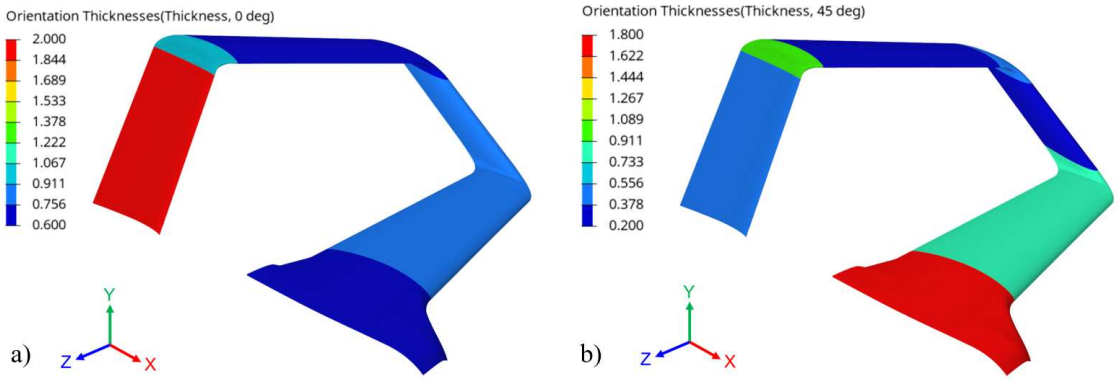

Figure 19: Contour plot and associated scale [mm] of the ply orientation thicknesses from the wing laminate optimization. 0 degrees is shown in a) and 45 degrees is shown in b).

In the wing sections that contain complex geometries where load paths are not necessarily straight, the 45-degree orientation (Figure 19b) appears to be more efficient and therefore is requested by the optimizer over the 0-degree orientation.

D. Design Comparison

It can be seen from Table 7 and Table 8 that the use of composite materials gives significant performance benefits relative to the aluminum designs. The total mass of the optimized composite design is 473.06kg, 54.1% less than that of the optimized aluminum design while meeting all design requirements.

Table 7: Quantitative comparison of the optimized mass for aluminum and composite wing designs.

Performance Measure	Aluminum	Composite
Mass [kg]	381.0	177.2 **(-53.49%)**
Safety Factor []	1.467	1.416
Maximum Displacement [mm]	88.17	192.7 **(+118.5%)**

Table 8: Quantitative comparison of the optimized mass for aluminum and composite fuselage designs.

Performance Measure	Aluminum	Composite
Mass [kg]	134.36	59.33 **(-55.8%)**
Safety Factor []	1.432	1.446
Max. Displacement [mm]	4.85	9.46 **(+95.1%)**

VI. Conclusions

This demonstration of a laminate optimization methodology applied to PAV design has shown the effectiveness of composite construction for UAM design. Table 7 and Table 8 show that the composite optimized structures are significantly lighter than the aluminum optimized structures. This gives strong evidence to suggest that composites are better suited to PAV design in comparison to conventional materials and should be used in future PAV development. All quantitative results show that while significant weight savings are achieved, the maximum displacement values are much larger for the composite designs in comparison to aluminum. No constraints on displacement were applied in the optimization, thus these designs are still admissible, however the composite designs' performance in this regard is lacking relative to the aluminum designs. In both the aluminum and composite designs, the thickness optimization requests the minimum thickness for many internal components – which shows that they could potentially be removed completely. The removal of several internal components (ie. ribs, spars, frames, stringers) would increase the risk of buckling in the skin due to the lack of support, but buckling is not a consideration for optimization currently and as such could not be mitigated automatically. Future work could include functionality to remove internal components and use buckling resistance as a design objective or constraint. While the composite

design performs significantly better than the aluminum design, a mixed-material design would result in further mass savings due to increased design freedom. A mixed material design could, for example, use a stiffer but heavier material (ex. steel) in high stress areas and a lighter but less stiff material (ex. LFPS) in low stress areas where strength/stiffness is less important. Finally, future work should implement composite optimization with more advanced methodologies, including free-size optimization, such that the full design freedom given by CFRP is used.

References

[1] Moore, M. D., "NASA Personal Air Transportation Technologies," SAE Technical Paper, 2006-02-2413, 2006. doi: 10.4271/2006-01-2413

[2] Johnson, W., Silva, C., "Observations from Exploration of VTOL Urban Air Mobility Designs," NASA ARC-E-DAA-TN60637, 2018.

[3] Clarke, M., Smart, J., Botero, E., Maier, W., Alonso, J. J., "Strategies for Posing a Well-Defined Problem for Urban Air Mobility Vehicles, *AIAA SciTech Forum*, San Diego, California, 2019. doi: 0.2514/6.2019-0818

[4] Krog, L., Tucker, A., Kemp, M., Boyd, R., "Topology Optimization of Aircraft Wing Box Ribs," *AIAA/ISSMO Multidisciplinary Analysis and Optimization Conference,* AIAA 2004-4481, Albany, NY, 2004.

[5] Krog, L., Tucker, A., Rollema, G., "Application of topology, size and shape optimization methods to optimal design of aircraft components," *Proceedings of 3rd Altair UK Hyperworks Users* Conference, 2002.

[6] Wong, J., Ryan, L., Kim, I. Y., "Design Optimization of Aircraft Landing Gear Assembly Under Dynamic Loading," Struct Multidisc Optim, Vol. 57, No. 3, 2018, pp. 1357, 1375. doi: 10.1007/s00158-017-1817-y

[7] Trivers, N. C., Carrick, C. A., Kim, I. Y., "Design Optimization of a Business Aircraft Seat Considering Static and Dynamic Certification Loading and Manufacturability," Struct and Multidisc Optim, published online 04 July 2020. doi: 10.1007/s00158-020-02650-z

[8] Li, C., Kim, I. Y., "Topology, Size and Shape Optimization of an Automotive Cross Car Beam," Journal of Automobile Engineering, Vol. 229, No. 10, 2015, pp. 1361, 1378. doi: 10.1177/0954407014561279

[9] Shrisvastava, S., Mohite, P. M., Yadav, T., Malaguadanavar, A., "Multi-objective Multi-laminate Design and Optimization of a Carbon Fibre Composite Wing Torsion Box Using Evolutionary Algorithm," Composite Structures, Vol 185, 2018, pp. 132-147.

[10] Kupchanko, L., Roper, S. W. K., Lee, H., Huh, M., Kim, I. Y., "A Comparison of Lightweight Design Concepts of a Passenger Aircraft Seat Using Topology and CFRP Laminate Optimization," *CSME Congress*, Charlottetown, PE, 2020. doi: 10.32393/csme.2020.104

[11] Hendricks, E. S., Falck, R. D., Gray, J. S., Aretskin-Hariton, E. D., Ingraham, D. J., Chapman, J. W., Schnulo, S. L., Chin, J. C., Jasa, J. P, Bergeson, J. D., "Multidisciplinary Optimization of a Turboelectric Tiltwing Urban Air Mobility Aircraft", *AIAA Aviation Forum,* Dallas, Texas, 2019. doi: 10.2514/6.2019-3551

[12] Metals Handbook, Vol. 2 – Properties and Selection: Nonferrous Alloys and Special-Purpose Materials, ASM International 10th Ed. 1990.

[13] Korea Institute of Carbon Convergence Technology (KCTECH)

[14] Federal Aviation Administration, "Airworthiness Standards: Normal, Utility, Acrobatic, And Commuter Category Airplanes," FAA 14 CFR 23.561, 2002, URL: https://www.govinfo.gov/content/pkg/CFR-2002-title14-vol1/pdf/CFR-2002-title14-vol1sec23-561.pdf